

# Opto-Electronic Science

ISSN 2097-0382

CN 51-1800/O4

## Unraveling the efficiency losses and improving methods in quantum dot-based infrared up-conversion photodetectors

Jiao Jiao Liu, Xinxin Yang, Qiulei Xu, Ruiguang Chang, Zhenghui Wu and Huaibin Shen

**Citation:** Liu JJ, Yang XX, Xu QL, et al. Unraveling the efficiency losses and improving methods in quantum dot-based infrared up-conversion photodetectors. *Opto-Electron Sci* **3**, 230029 (2024).

<https://doi.org/10.29026/oes.2024.230029>

Received: 25 August 2023; Accepted: 18 December 2023; Published online: 21 March 2024

## Related articles

### Highly efficient emission and high-CRI warm white light-emitting diodes from ligand-modified CsPbBr<sub>3</sub> quantum dots

Dongdong Yan, Shuangyi Zhao, Yubo Zhang, Huaxin Wang, Zhigang Zang

*Opto-Electronic Advances* 2022 **5**, 200075 doi: [10.29026/oea.2022.200075](https://doi.org/10.29026/oea.2022.200075)

### Giant magneto field effect in up-conversion amplified spontaneous emission via spatially extended states in organic-inorganic hybrid perovskites

Tangyao Shen, Jiajun Qin, Yujie Bai, Jia Zhang, Lei Shi, Xiaoyuan Hou, Jian Zi, Bin Hu

*Opto-Electronic Advances* 2022 **5**, 200051 doi: [10.29026/oea.2022.200051](https://doi.org/10.29026/oea.2022.200051)

### Applications of lasers: A promising route toward low-cost fabrication of high-efficiency full-color micro-LED displays

Shouqiang Lai, Shibiao Liu, Zilu Li, Zhening Zhang, Zhong Chen, Rong Zhang, Hao-Chung Kuo, Tingzhu Wu

*Opto-Electronic Science* 2023 **2**, 230028 doi: [10.29026/oes.2023.230028](https://doi.org/10.29026/oes.2023.230028)

### Switching of K-Q intervalley trions fine structure and their dynamics in n-doped monolayer WS<sub>2</sub>

Jiajie Pei, Xue Liu, Andrés Granados del Águila, Di Bao, Sheng Liu, Mohamed-Raouf Amara, Weijie Zhao, Feng Zhang, Congya You, Yongzhe Zhang, Kenji Watanabe, Takashi Taniguchi, Han Zhang, Qihua Xiong

*Opto-Electronic Advances* 2023 **6**, 220034 doi: [10.29026/oea.2023.220034](https://doi.org/10.29026/oea.2023.220034)

More related article in Opto-Electronic Journals Group website 

 Opto-Electronic  
Science

<http://www.ojournal.org/oes>



 OE\_Journal



Website

DOI: [10.29026/oes.2024.230029](https://doi.org/10.29026/oes.2024.230029)

# Unraveling the efficiency losses and improving methods in quantum dot-based infrared up-conversion photodetectors

Jiao Jiao Liu, Xinxin Yang, Qiulei Xu, Ruiguang Chang, Zhenghui Wu<sup>✉</sup> and Huaibin Shen\*

Quantum dot-based up-conversion photodetector, in which an infrared photodiode (PD) and a quantum dot light-emitting diode (QLED) are back-to-back connected, is a promising candidate for low-cost infrared imaging. However, the huge efficiency losses caused by integrating the PD and QLED together hasn't been studied sufficiently. This work revealed at least three origins for the efficiency losses. First, the PD unit and QLED unit usually didn't work under optimal conditions at the same time. Second, the potential barriers and traps at the interconnection between PD and QLED units induced unfavorable carrier recombination. Third, much emitted visible light was lost due to the strong visible absorption in the PD unit. Based on the understandings on the loss mechanisms, the infrared up-conversion photodetectors were optimized and achieved a breakthrough photon-to-photon conversion efficiency of 6.9%. This study provided valuable guidance on how to optimize the way of integration for up-conversion photodetectors.

**Keywords:** infrared colloidal quantum dots; up-conversion photodetector; integration loss; interconnection; voltage allocation

Liu JJ, Yang XX, Xu QL et al. Unraveling the efficiency losses and improving methods in quantum dot-based infrared up-conversion photodetectors. *Opto-Electron Sci* 3, 230029 (2024).

## Introduction

Infrared photodetectors (PDs) promise lots of applications in the field of bio-sensing and imaging<sup>1-5</sup>. Traditional infrared imagers are usually constructed by bonding an infrared PD with each pixel in a thin film transistor (TFT)-based active-matrix backplane<sup>6</sup>. A feasible way to avoid the costly pixilation is to use infrared up-conversion photodetector, in which an infrared photodetector (PD) and a light-emitting diode (LED) with large effective areas are back-to-back connected<sup>7,8</sup>. With excitations from infrared signals, the holes from photoexcita-

tion in the PD unit and electrons from external injection are radiatively recombined in the LED unit, so that the infrared up-conversion photodetectors emit visible light. Without infrared signals, the up-conversion photodetectors keep dark. Therefore, infrared imaging based on up-conversion photodetectors neither needs discrete pixels, nor the expensive indium pillar welding process<sup>9</sup>. In early days, the PD part or LED part in up-conversion photodetectors is based on inorganic epitaxial materials, which need costly fabrication procedures<sup>10,11</sup>. Promising low-cost materials for PD and LEDs include organic

Key Laboratory for Special Functional Materials of Ministry of Education, National & Local Joint Engineering Research Centre for High-efficiency Display and Lighting Technology, School of Materials, Henan University, Kaifeng 475004, China.

\*Correspondence: ZH Wu, E-mail: wuzhenghuihk@henu.edu.cn; HB Shen, E-mail: shenhuaibin@henu.edu.cn

Received: 25 August 2023; Accepted: 18 December 2023; Published online: 21 March 2024



**Open Access** This article is licensed under a Creative Commons Attribution 4.0 International License.

To view a copy of this license, visit <http://creativecommons.org/licenses/by/4.0/>.

© The Author(s) 2024. Published by Institute of Optics and Electronics, Chinese Academy of Sciences.

semiconductors and colloidal semiconductor quantum dots. However, organic up-conversion PD is usually fabricated with complicated thermal evaporation deposition, since we can hardly find orthogonal solvents for the multiple organic functional layers<sup>12</sup>. Recently, lead sulfide (PbS) and cadmium selenide (CdSe) colloidal quantum dots (CQDs) have been reported to work as infrared active materials and visible emitting materials in infrared up-conversion photodetectors, respectively. CQDs show advantages of low-cost solution processabilities and excellent stability in air<sup>13–16</sup>. Particularly, PbS CQDs are increasingly used in photovoltaics<sup>17–19</sup>, light emitting diodes (LEDs)<sup>20,21</sup> and photodetection<sup>22,23</sup>.

In recent decades, quite a few works reported up-conversion photodetectors based on low cost novel semiconductors such as organics and CQDs. So et al. applied organics in both the PD unit and LED unit of an up-conversion photodetector, though it was fabricated via multiple runs of thermal evaporation<sup>24</sup>. Under high working bias of about 12 V, the up-conversion photodetectors showed photon-to-photon conversion efficiency ( $\eta_{pp}$ ) of about 1.3%. Since 2019, several works reported all-solution processed up-conversion photodetectors with both PD and LED units based on CQDs<sup>21,25,26</sup>. When PbS-based PD and CdSe-based QLED work alone, the photon-to-electron conversion efficiency (*IPCE*) of the PD and the electron-to-photon conversion efficiency (*EQE*) the QLED can be as high as 104%<sup>27</sup> and 25%<sup>28</sup>, respectively. However, when the CQDs-based PD and QLED were integrated into the up-conversion photodetectors, the highest reported  $\eta_{pp}$  was only 6.5%, which was much smaller than the *IPCE*  $\times$  *EQE* product (i.e., 104%  $\times$  25% = 2500%). In previous works, the efficiency of the all-CQD up-conversion devices was improved by adjusting the optimized working voltages of the QLED unit<sup>29</sup> or the optimized thickness of the infrared absorbing layer in the PD unit (our previous work)<sup>30</sup>. However, these improvements were just based on empirical experiences and experimental attempts, and there haven't been sufficient understandings on the origins of the huge efficiency losses after the high-performance PDs and QLEDs are integrated together to form up-conversion photodetectors. To improve the performance of up-conversion photodetectors further and realize their practical applications, it's important to fully understand the huge efficiency losses and how the PD and QLED units constrain each other in the up-conversion photodetectors.

In this work, high-efficiency up-conversion photode-

tectors based on PbS CQDs infrared absorber and Cd-based CQD red emitters are fabricated. The investigation of the efficiency loss started with the comparisons between the up-PDs with different interconnections, i.e., Poly(9,9-dioctylfluorene-alt-N-(4-sec-butylphenyl)-diphenylamine) (TFB) and Poly[bis(4-phenyl)(2,4,6-trimethylphenyl)amine] (PTAA). TFB and PTAA are also popular hole transport layers (HTL) in QLEDs. When PTAA or TFB were used as HTL in Cd-based QLEDs, the turn-on voltages were similar, though their energy levels showed some differences<sup>16</sup>. On the other hand, turn-on voltages of the up-conversion photodetectors with TFB or PTAA interconnection layers showed significant differences. This suggested that the effective biases allocated onto the QLED unit of the up-conversion devices were affected by the interconnection layers. The mechanisms of voltage allocations among the PD unit, the interconnection, and the QLED unit in up-PDs were discussed. Under low bias, effective bias allocated onto the PD unit was nearly zero, leading to extremely low *IPCE* of the PD unit. In addition, there was serious accumulation and quenching of photogenerated holes in the up-conversion photodetectors with TFB interconnection under low bias, due to the high potential barriers at the interconnection. Though high *IPCE* was achieved and potential barrier at the interconnection was fully overcome with high working bias in up-conversion photodetectors, the efficiency roll-off of the QLED unit with high effective allocated bias still induced high integration loss. In addition, the discussions and analysis quantified the loss contributed by the absorption of visible emission in the PD unit, which usually accounted for over 60% of the total losses. Based on the understandings on the loss mechanisms, the infrared up-conversion photodetectors were optimized and achieved a breakthrough photon-to-photon conversion efficiency of 6.9%, exceeding the previously reported highest efficiency. This work provided comprehensive understanding on optimizing the way of integration in up-conversion photodetectors, rather than optimizing the PDs or QLEDs before they are integrated.

## Results and discussions

Figure 1(a) schematically illustrated the typical device structure of the up-conversion photodetector in this work. Lead sulfide (PbS) CQDs with tetrabutylammonium iodide (TBAI) ligands showed n-type carrier transport, and those with 1,2-ethanedithiol (EDT) ligands

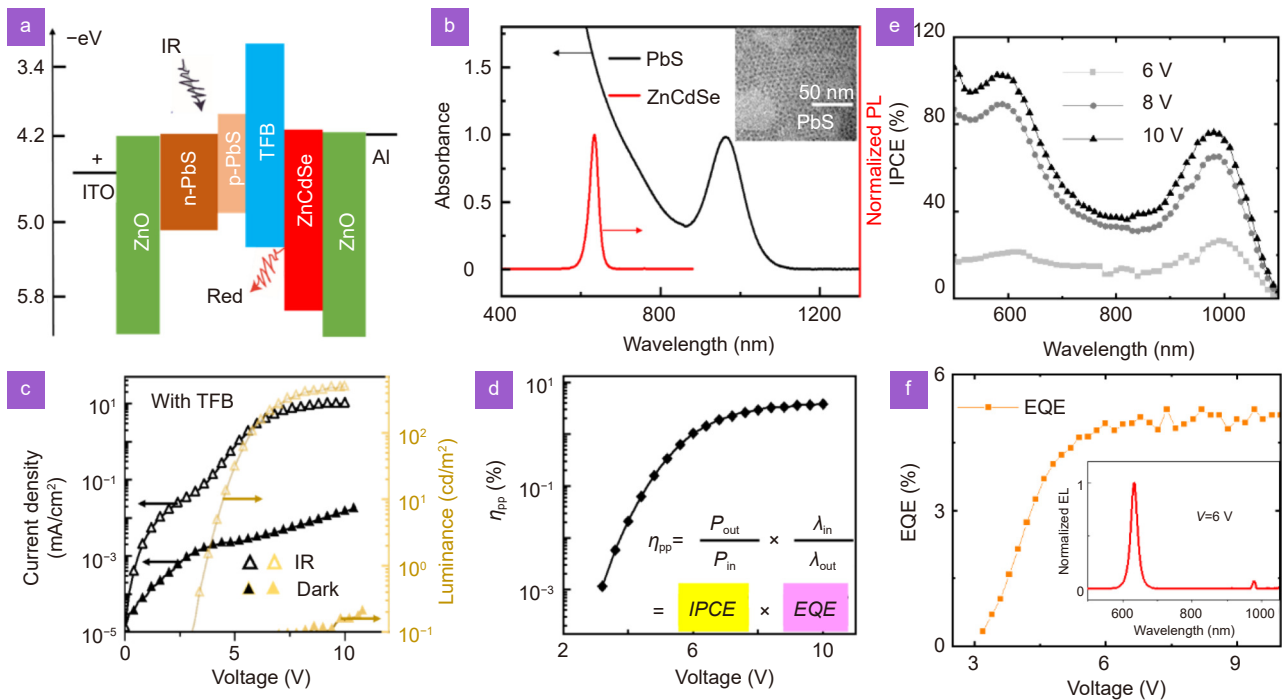


**Fig. 1 |** (a) Schematic picture showing the device structure of quantum dot-based up-conversion photodetector. (b) The PL spectrum of ZnCdSe QDs and spectral absorbance of PbS QDs, the inset shows the TEM image of PbS QDs. (c) The  $J$ - $V$ - $L$  characteristics of the up-conversion photodetector in dark and under  $18 \text{ mW/cm}^2$  980 nm illumination. (d)  $\eta_{pp}$  of the up-conversion photodetector with its definition and physical interpretation shown in the inset. (e) The spectral  $IPCE$  of the up-conversion device under different applied bias. (f) The  $EQE$  of the up-conversion device; the inset shows the EL spectrum of the up-conversion device with 6 V applied bias and infrared illumination.

show p-type carrier transport. According to previous studies, the valence bands (VB) of the n-type and p-type PbS CQDs in our devices were about  $-5.4 \text{ eV}$  and  $-4.9 \text{ eV}$ , respectively<sup>31</sup>. The difference between their fermi levels was about  $0.4 \text{ eV}$ <sup>31</sup>, which determined the maximum photovoltages of this p-n junction. On the other side of the up-conversion photodetectors, it was a QLED based on ZnCdSe/ZnS red emitting CQDs. TFB layer worked as hole collection layer in the PD unit, while it worked as HTL in the QLED unit. The layer of ZnO at the ITO side worked as electron extraction layer in the PD unit with infrared illumination, while it worked as hole blocking layer in the up-conversion photodetector in dark. The ZnO at the Al side worked as electron injection layer in the QLED unit. The photoluminescence (PL) spectrum of ZnCdSe/ZnS CQDs and the spectral absorbance of the PbS CQDs were shown in Fig. 1(b). The luminous efficacy is about  $144 \text{ lm/W}$  at the emission peak of  $633 \text{ nm}$ , which was explained in details in Section S1 in Supplementary information. Light emitted from planar QLED usually shows Lambertian spatial optical distribution. Then, the luminance ( $L$ ) of the up-conversion photodetectors and QLED were related to the emitting power intensity ( $P_{out}$ ) by the following equation,

$$P_{out} = \frac{\pi \cdot L}{144 \text{ lm/W}}, \quad (1)$$

whose derivation was shown in Section 1 in Supplementary information. The absorption peak of PbS CQDs was around  $980 \text{ nm}$ . Since it was difficult to directly measure the power density of the obliquely incident infrared light, the power density of incident infrared light was calculated from the directly measured  $IPCE$  and photocurrent density of the up-conversion photodetectors.

The current density – voltage – luminance ( $J$ - $V$ - $L$ ) characteristics of the up-conversion photodetector with TFB as interconnection were shown in Fig. 1(c). The PD unit in this device worked in typical photovoltaic mode with minimal photoconductive gains, since the photocurrent showed a stable saturation value under high bias. In dark, the up-conversion device can hardly emit red light. On the other hand, the up-conversion device with TFB as interconnection emitted red light when the applied bias increased to over  $3.2 \text{ V}$  under infrared illumination. The key figure-of-merits for the up-conversion device, i.e.,  $\eta_{pp}$  vs. voltage, was shown in Fig. 1(d).  $\eta_{pp}$  increased as applied bias increased and approached to a saturation value of  $3.7\%$  at  $10 \text{ V}$ , which was comparable to the previously reported  $\eta_{pp}$  for PbS CQDs-based



up-conversion device without photoconductive gains<sup>21</sup>. Here,  $\eta_{pp}$  characterizes the ratio of the number of emitted visible photons to the number of incident infrared photons, which is calculated by Eq. (2):

$$\eta_{pp} = \frac{P_{out}/\frac{hc}{\lambda_{in}}}{P_{in}/\frac{hc}{\lambda_{out}}} = \frac{P_{out}}{P_{in}} \times \frac{\lambda_{in}}{\lambda_{out}}, \quad (2)$$

where  $P_{in}$  is the infrared incident power density,  $h$  is Planck constant,  $c$  is speed of light,  $\lambda_{in}$  is the wavelength of the incident light,  $\lambda_{out}$  is the wavelength of the visible emitted light. Since the up-conversion device can work as either a PD or a QLED,  $\eta_{pp}$  can be decomposed into two components as shown in Eq. (3),

$$\eta_{pp} = IPCE \times EQE, \quad (3)$$

please be noted that the *IPCE* or *EQE* here refers to the quantum efficiency of the up-conversion device when it works as a PD or a QLED, rather than the quantum efficiency of the PD or QLED before it is integrated into the up-conversion device. All the three parameters in Eq. (3) depend on the total bias across the up-conversion device. Figure 1(e) showed the measured spectral *IPCE* of the up-conversion device when it worked as a photodetector. The *IPCE* of the up-conversion device with 10 V bias and 980 nm incident light was about 76%. Figure 1(f) showed the measured *EQE* of the up-conversion device was about 5.1% when it worked as a light-emitting diode with high bias. This suggested  $\eta_{pp} = 76\% \times 5.1\% = 3.88\%$ , which was consistent with the measured  $\eta_{pp}$  shown in Fig. 1(d). The inset in Fig. 1(f) showed the electroluminescence spectrum of the up-conversion device with 6 V bias under infrared illumination. It consisted of a strong emission with peak at 633.5 nm and a weak emission with peak at 978 nm. Since the infrared peak only had a full width at half maximum of 6 nm, we thought the peak was due to the reflected incident 978 nm laser illumination, rather than the electroluminescence (EL) of the PbS CQD layers.

PDs and QLEDs with the same materials and process engineering used for the up-conversion devices were fabricated. In details, the device structure of the independent QLED followed ITO/ PEDOT:PSS/ TFB or PTAA/ ZnCdSe/ZnS CQDs/ ZnO/ Al, and the device structure of the independent PD followed ITO/ ZnO/ n-PbS CQDs/ p-PbS CQDs/ Au, where PEDOT:PSS is for Poly(3,4-ethylenedioxythiophene) polystyrene sulfonate. The *J-V-L* and *EQE* vs. voltage characteristics of the

QLED were shown in Fig. 2(a, b). No matter TFB or PTAA is used as HTLs, the turn-on voltage of the independent QLED was only about 1.8 V, much lower than that of the up-conversion devices. Lots of previous works also indicated that the hole injection barriers were minimal in QLEDs no matter TFB or PTAA is used as HTL<sup>16,32</sup>. As bias exceeded 2.6 V, *EQE* of QLED continue to drop with increasing bias, while  $\eta_{pp}$  of up-conversion device kept rising as the bias increased to 10 V. The distinct bias-dependences between the *EQE* in independent QLEDs and  $\eta_{pp}$  in up-PDs might be caused by the following two possible reasons: a) improvements in *IPCE* of the PD unit as bias increased compensated the decrease in the *EQE* of the QLED unit; b) the effective bias allocated to the QLED unit doesn't increase linearly with the increase of total bias across the up-conversion devices. Whether the PD or QLED units integrated into the up-conversion devices worked optimally was directly determined by the effective biases allocated to them. Therefore, we started the investigation of the efficiency losses in up-conversion devices by understanding the voltage allocations among the PD unit, interconnection and QLED unit. As shown in Fig. 2(c), though the independent QLEDs with TFB or PTAA showed the same turn-on voltage, the turn-on voltage of the up-conversion device with PTAA under infrared illumination was only about 2.2 V, while it was about 3.2 V if TFB was used as interconnection. Before in-depth analysis on the interaction between the interconnection, the PD unit and QLED unit, the characteristics of the independent infrared PD also needed to be understood further. As shown in Fig. 2(d), the open circuit voltage ( $V_{oc}$ ) of the independent PD under 18 mW/cm<sup>2</sup> 980 nm illumination was about 0.37 V, which was consistent with the off-set between the fermi levels of n-type PbS and p-type PbS used in this work. In up-conversion devices,  $V_{oc}$  of the PD unit together with the applied bias drove the photocurrent and inject photogenerated holes into the QLED unit. The dependence of the photocurrent of the independent PD on effective bias ( $V_{eff} = V_{oc} + \text{applied bias}$ ) was shown by the black circles in Fig. 2(e). The photocurrent vs. effective bias of a typical photovoltaic PD without the problems of exciton dissociation usually complies with Hetch formula. Due to high dielectric constant of CQDs and excellent electronic coupling between the PbS CQDs with short ligands, the exciton dissociation is usually 100% even without any help from external bias<sup>33,34</sup>. Hetch formula was expressed as below,

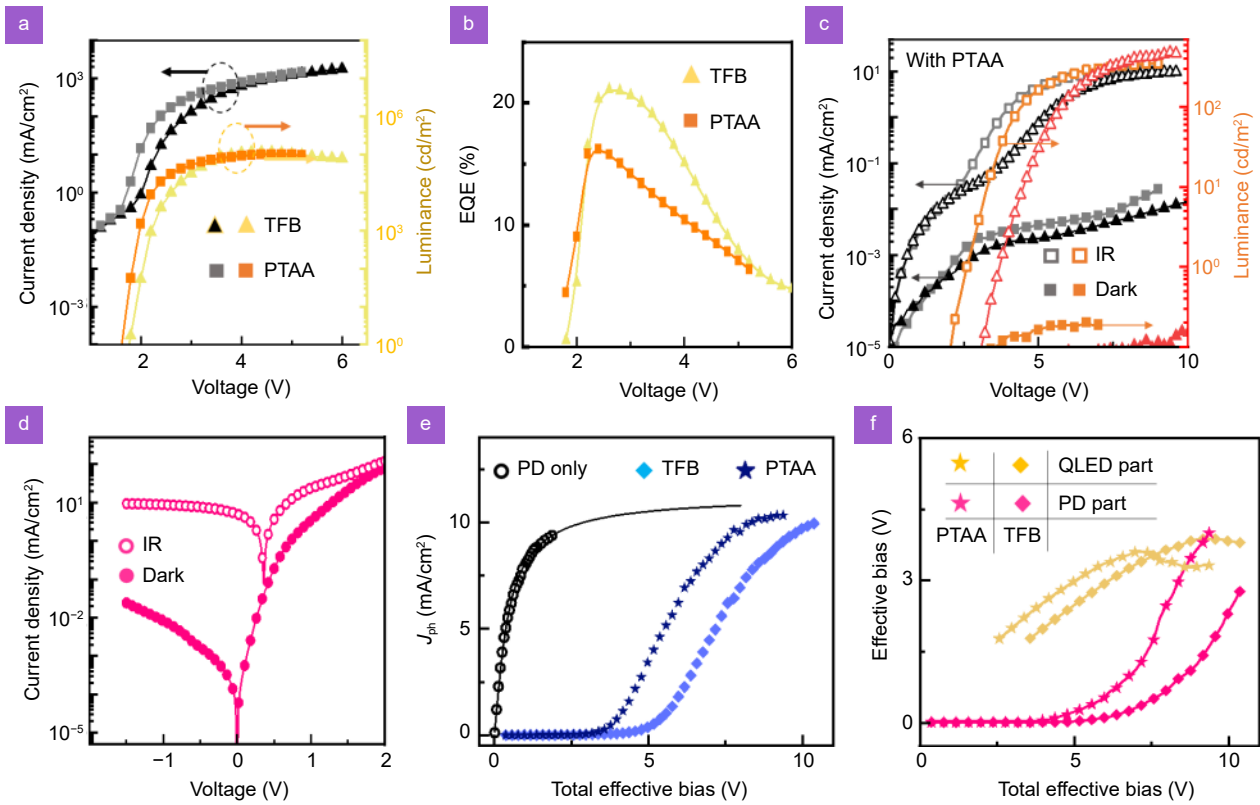


**Fig. 2 |** (a) The  $J$ - $V$ - $L$  characteristics and (b) EQE of ZnCdSe-based QLEDs with TFB or PTAA as hole transport layer. (c) The  $J$ - $V$ - $L$  characteristics of the up-conversion device with TFB replaced by PTAA as interconnection layer. (d) The  $J$ - $V$  characteristics of the PbS-based PDs in dark or under 18 mW/cm<sup>2</sup> 980 nm illumination. (e) The photocurrent vs. effective bias characteristics of PbS-based PD and up-conversion devices with TFB or PTAA as interconnection layers, solid line represents the fitted photocurrent with Hetch formula. (f) The effective biases across the PD unit and QLED unit in the up-conversion device with TFB or PTAA as interconnection layers.

$$J_{\text{ph}}(V_{\text{eff}}) = J_{\text{sat}} \frac{\mu\tau V_{\text{eff}}}{dd'} \left[ 1 - \exp\left(-\frac{dd'}{\mu\tau V_{\text{eff}}}\right) \right], \quad (4)$$

where  $d$  was the total thickness of PbS CQDs, and was measured to be about 180 nm;  $d'$  was the carrier transport distance, and usually is approximated as  $d/2$  on average;  $\mu\tau$  was the mobility-lifetime product. The physical interpretations of  $\mu\tau$  were elaborated in ref.<sup>10,11</sup>. The experimental  $J_{\text{ph}}(V_{\text{eff}})$  of the independent PD fitted well with Eq. (3), as shown by the solid black line in Fig. 2(e). The details of the fitting parameters are shown in Section S2 in Supplementary information. According to the fitting with Hetch formula, the saturated photocurrent density was about  $(11.3 \pm 0.2)$  mA/cm<sup>2</sup> under 18 mW/cm<sup>2</sup> infrared illumination. Saturated photocurrent was achieved when the external bias was large enough to extract out all of the photogenerated carriers, i.e., 100% internal quantum efficiency. Therefore, the absorption percentage ( $\eta_{\text{abs}}$ ) at 980 nm can be estimated by:

$$\eta_{\text{abs}} = J_{\text{sat}} / P_{\text{in}} \times hc / \lambda e, \quad (5)$$

where  $h$  is Planck constant,  $c$  is speed of light,  $e$  is elementary charge. Then the absorption percentage was es-

timated to be about 80%. This estimated value was consistent with numerous precious works about PbS-based solar cells or photodiodes, which suggested that the highest IPCE (i.e.,  $\eta_{\text{abs}}$ ) at the first excitonic absorption peak position of PbS-based photodiodes with planar multi-layer structure was about 80%<sup>30,33,34</sup>. The  $J_{\text{ph}} - V$  characteristics of the up-conversion photodetectors with TFB or PTAA interconnection were shown by the stars and diamonds in Fig. 2(e). Not only the 980 nm incident light, but also the red emission of QLED part contributed to  $J_{\text{ph}}$  in the up-conversion devices. On the other hand, there might be slight loss of optical absorption due to the weak absorption and scattering in TFB and ZnCdSe layers in up-conversion photodetectors. To simplify the analysis, the absorption percentages in independent PD and in up-conversion devices were assumed to be similar if the thicknesses of PbS layers were similar. This would introduce an error of ~4% at most for the following quantitative analysis, which was explained in more details in Section 2 in Supplementary information. With sufficient large bias, the photocurrent densities in

the up-conversion photodetector also approached to the similar saturated photocurrent.

By equating  $J_{ph}(V)$  for the independent PD to the  $J_{ph}(V)$  for up-conversion devices, the relationship between the effective bias allocated to the PD unit ( $V_p$ ) and the total bias across the whole up-conversion device ( $V_{total}$ ) was estimated and shown by the pink symbols in Fig. 2(f). The results in Fig. 2(f) showed that the voltage allocated onto the PD unit in the up-PD was very small when  $V_{total}$  is less than 6 V. With low effective bias across the PD unit, the IPCE of the up-PD was very low, which is responsible for the low  $\eta_{pp}$  of up-conversion devices with low working bias. The effective biases allocated onto the three units in up-PD, i.e., the PD unit, the interconnection, and QLED unit, were determined by the resistances of the three parts connected in series. Under illumination, the resistance of the PD unit was small due to large amounts of photogenerated carriers. On the other hand, the resistances of the interconnection and QLED unit were very large when the up-conversion device was just turned on under low applied bias. The interconnection was equivalent to a Schottky diode, while the QLED unit was a typical p-i-n junction diode. Since the current flowing through the whole device was very small ( $< 10$  mA/cm<sup>2</sup>), carrier transport in both interconnection and QLED unit didn't run into the space charge limited regions. Both resistances of the interconnection and QLED unit were dominated by the diode resistances and decrease exponentially as bias increases. The exponent was determined by  $e/(nkT)$ , where  $e$  was the elementary charge,  $n$  was the ideality factor of the two diodes, and  $kT$  was the Boltzmann-temperature product. Previous studies on the  $J$ - $V$  characteristics of diodes based on low-mobility ( $\ll 1$  cm<sup>2</sup>·V<sup>-1</sup>·s<sup>-1</sup>) materials<sup>35,36</sup> showed that the ideality factor was mainly affected by the carrier transport through the diodes. According to the understandings on the carrier injection and transport in QLEDs with ZnO electron transport layer<sup>37</sup>, the series resistance of the QLED unit is mainly contributed by the slow hole transport, since the electrons injected from the ZnO side would prevent more electron injections through coulombic repulsion until they met holes injected from HTL. Here, we assume that both resistances of the interconnection and QLED unit in up-PD decreased exponentially with about the same exponent  $e/nkT$  as total applied bias increased, leading to equal allocation of additional voltages onto the interconnection and QLED unit. More discussions on the resistances of the intercon-

nection and QLED unit were showed in Section S3 in Supplementary information. In up-conversion device with TFB, the device was turned on with 3.2 V applied bias (i.e., 3.57 V total effective bias), among which  $\sim 1.8$  V was allocated onto the QLED unit to turn on the device, nearly 0 onto the PD unit, and the left ( $\sim 1.77$  V) was allocated onto the interconnection. In up-conversion device with PTAA as interconnection, the device was turned on with 2.2 V applied bias (i.e., 2.57 V total effective bias), among which  $\sim 1.7$  V was allocated onto the QLED unit, nearly 0 onto the PD unit, and the left ( $\sim 0.87$  V) was allocated onto the interconnection. As the total bias increased, the additional voltage available for the interconnection and QLED unit was equally allocated. Then the effective biases across the QLED unit in up-conversion device with TFB or PTAA as interconnection were derived and shown in Fig. 2(f).

Since there hasn't been a feasible way to monitor the effective biases allocated onto different units in up-conversion devices, the voltage allocations among the PD unit, QLED unit and the interconnection were explained in more details by the equivalent circuit model shown in Fig. 3(a). The modeling circuit for the PD unit was exactly the classical circuit for solar cells. The interconnection and QLED unit were regarded as the loads of the PD unit. Shunt resistances ( $R_{SH}$ ) of the three units took the leakage currents into accounts. Series resistances ( $R_{S-p}$ ,  $R_{S-int}$ ,  $R_{S-Q}$ ) of the three units were the internal resistances determined by the carrier transport characteristics. The diode resistance of the interconnection part is contributed by the carrier injection barriers at the PD/HTL and HTL/QLED interfaces. More details about the diode resistance is discussed in Section S3 in Supplementary information. In dark, photocurrent ( $J_{ph}$ ) is zero, leaving the diodes in the PD unit and QLED unit connected back-to-back. Under illumination and negative applied bias (negative to the PD unit, but positive to the whole up-conversion device), photocurrent mainly flowed through the three series resistances and the diode resistances in the interconnection and QLED unit, but not through the diode resistance in the PD unit. With small flowing photocurrent or before the up-conversion device was turned on, the diode resistances were much larger than all the three series resistance in PD unit, the interconnection and QLED unit. Therefore, the voltages allocated onto the PD unit, the interconnection and QLED unit were determined by the series resistance of the PD, the diodes resistances of the QLED unit and

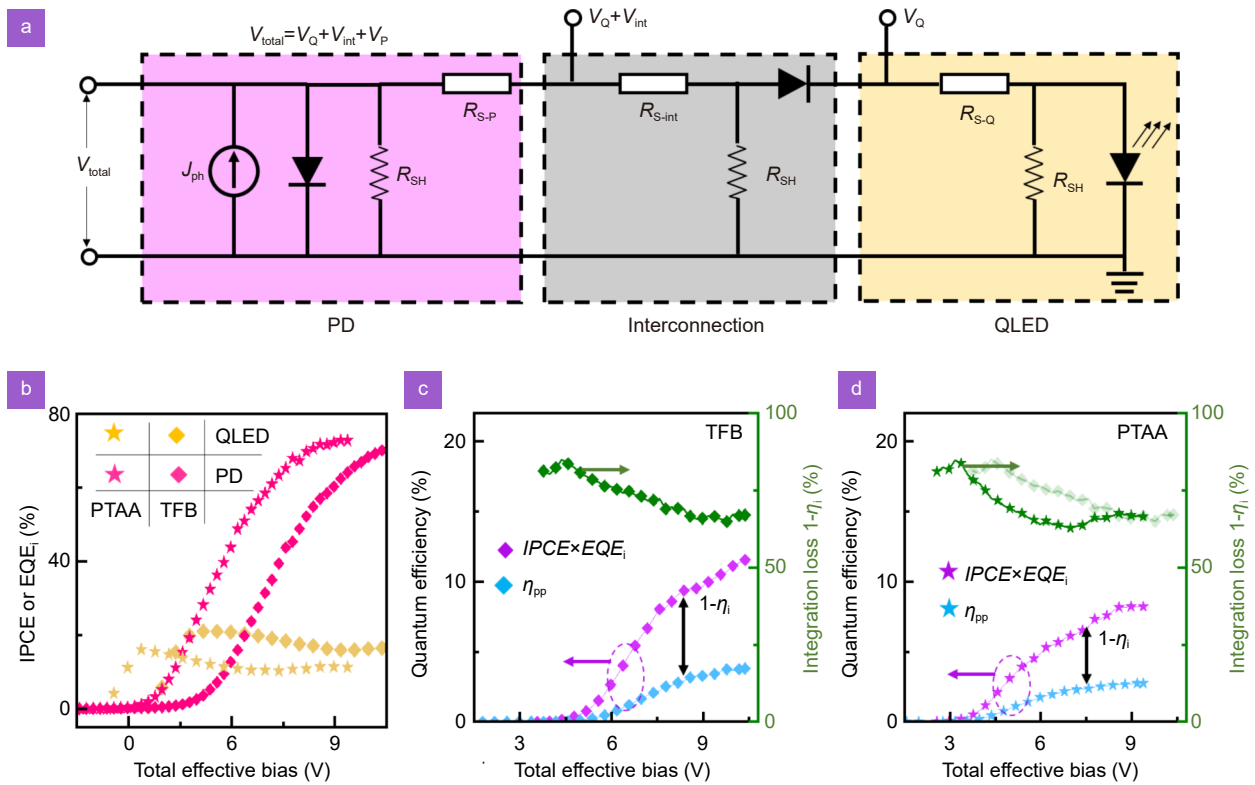


**Fig. 3 |** (a) Equivalent circuit explaining the voltage allocations in up-conversion devices. (b) The quantum efficiencies of independent PD and QLED under working conditions simulating those of the PD unit and QLED unit in up-conversion devices. (c–d) The comparisons between the products of effective  $IPCE \times EQE_i$  and the measured  $\eta_{pp}$  of up-conversion device with TFB and PTAA as interconnection layers, the green curves show the gaps between  $IPCE \times EQE_i$  product and  $\eta_{pp}$ , representing the integration losses.

interconnection. When the total applied bias is small, the effective bias allocated onto the PD unit was minimal due to the too large diode resistances in the QLED unit and the interconnection. Only when the diodes resistances in QLED unit and the interconnection decreased to about the same order of the series resistances under large total applied bias, could the PD unit obtain enough effective bias to generate high photocurrent and  $IPCE$ .

Figure 2(f) depicted the actual working conditions of the QLEDs when they were integrated into the up-conversion devices. This allowed us to examine the performances of the independent QLEDs when they simulating the working conditions of the QLED units in up-PDs. Based on the  $EQE$  vs. voltage characteristics of the independent QLEDs shown in Fig. 2(b), the quantum efficiencies of the independent QLEDs but under the same working conditions of the QLED units in up-conversion devices were derived, which was shown by the  $EQE_i$  vs. total effective bias in Fig. 3(b). Then,  $\eta_{pp}$  can be further decomposed into Eq. (6):

$$\eta_{pp} = IPCE \times EQE = IPCE \times EQE_i \times \eta_i, \quad (6)$$

please be noted that  $EQE$  was the efficiency of the up-

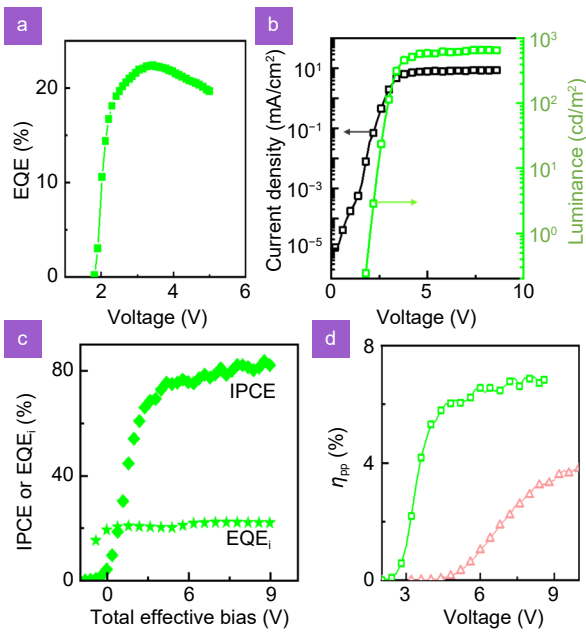
conversion device when it worked as an emitting diode, while the  $EQE_i$  was the efficiency of an independent QLED when it simulating the working conditions of the QLED unit in up-conversion device.  $\eta_i$  represented integration efficiency, i.e.,  $(1 - \eta_i)$  meant the efficiency loss due to integrating the PD and QLED into the up-conversion device. From Fig. 3(b), we can see that optimal working conditions of the QLED unit were mainly achieved when the up-conversion device worked under low bias. As total bias across the whole up-conversion device increased,  $IPCE$ s of the PD units keep increasing, while the QLED units suffered significantly from the efficiency roll-offs on the other hand. As shown in Fig. 3(c, d), the  $IPCE \times EQE_i$  products increased with total effective bias. However, the  $IPCE \times EQE_i$  product at high bias was still far below the  $\max-IPCE \times \max-EQE_i$  (i.e.,  $80\% \times 22\%$  or  $\sim 17.6\%$ ), because the optimal working conditions for the PD unit and the QLED unit were not achieved with the same total effective bias. On the other hand, there was also large gap between the  $IPCE \times EQE_i$  product and the measured  $\eta_{pp}$  under any working biases. This gap was indicated by the integration loss  $(1 - \eta_i)$ .



Figure 3(c, d) compared the integration losses in up-conversion devices with TFB and PTAA as interconnections. The integration loss under low bias ( $< 6$  V) in device with PTAA was significantly lower than that in device with TFB due to the lower potential barrier at the PTAA interconnection. Here is a short summary on the carrier losses caused by integrating the PD unit and QLED unit: with low total effective bias, large amounts of photogenerated carriers were recombined in the PD unit, resulting in low *IPCE* for the PD unit and low  $\eta_{pp}$  in up-conversion device. The bimolecular recombination between the photogenerated electrons and holes was highly efficient in the PD unit when the effective bias allocated onto the PD unit was small. On the other hand, the recombination between the photogenerated holes and the trapped electrons or electrons escaped from the QLED unit might be also highly efficient when the potential barrier at the interconnection was high, leading to high integration loss ( $1 - \eta_i$ ) under low working bias ( $< 6$  V). Under high working bias, efficiency roll-off of the QLED unit was an important limiting factor for the  $\eta_{pp}$  in up-conversion device. No matter TFB or PTAA interconnections were used, the integration losses were similar under high working bias, since the potential barriers at the interconnection were both fully overcome. However, the integration loss was still over 65% even if the interconnection barriers were fully overcome by large applied bias ( $\sim 10$  V). The 65% integration losses under high bias were mainly caused by the absorption of the visible emission in PD unit. In addition, the non-radiative recombination loss due to unbalanced injections of photogenerated holes and external electrons in the QLED unit might be another reason for the integration loss under high bias. Our previous work<sup>30</sup> investigated the absorption of visible emission and non-radiative recombination loss in up-conversion photodetectors in details. Since the up-conversion devices with TFB or PTAA showed similar optical structures, the losses due to absorption of visible emission should also be similar in two devices.

Based on the understanding of the loss mechanisms in quantum-dot based infrared up-conversion devices, several approaches have been applied to improve their performances. The most serious loss was contributed by the absorption of the emitted visible light in PbS layers. In our just published work, we showed that decreasing the total thickness of PbS layers from 180 nm to 140 nm im-

proved  $\eta_{pp}$  from 3.6% to 4.5%<sup>30</sup>. Nevertheless, there is only limited improvement by tuning the thicknesses of PbS layers, since PbS quantum dots always shows strong absorption in visible spectrum. More efficient ways to mitigate the loss from re-absorption rely on developing more sophisticated optical structure, such as micro-cavity or plasmonic structure. On the other hand, the comparisons between the performances of up-conversion devices with TFB or PTAA interconnection layers already showed that HTL with higher highest occupied molecular orbital (HOMO) levels efficiently reduced the turn-on voltages and improved  $\eta_{pp}$  under low working bias. However, under high working bias  $\eta_{pp}$  was not improved by using PTAA with higher HOMO levels. This suggested that some interfacial properties other than interfacial barriers deeply affect the performances of quantum-dot based up-conversion devices. Our previous work explained how the carrier trapping and accumulation at the interfaces affect the performances of up-conversion devices. More comprehensive and profoundly understandings on the interfacial properties in up-conversion devices are desired. Another easy approach to improve the performance of up-conversion devices is to achieve a better matching between the PD unit and QLED unit. Since High *IPCE* must be achieved with high working bias in PD unit, better matching between the PD unit and QLED is usually achieved by integrating a QLED with less efficiency roll-offs. As shown in Fig. 4(a), the red QLED based on a new batch of CdSe/ZnS quantum dots with thicker shells showed much less efficiency roll-offs and kept *EQE*  $> 21\%$  until the bias increased to 4 V. When this QLED was integrated into the up-conversion devices, the max luminance was about 660 cd/m<sup>2</sup> with  $\sim 13.5$  mW/cm<sup>2</sup> infrared (980 nm) illumination, as shown in Fig. 4(b). Following the above similar methods, the *IPCE* and *EQE<sub>i</sub>* of this up-conversion device were calculated and shown in Fig. 4(c). It showed that the maxima values of *IPCE* and *EQE* were achieved at the same time when the device worked under bias of  $> 6$  V. Finally, the improved match between the PD unit and QLED unit, together with optimized PbS layers, resulted in a  $\eta_{pp}$  of 6.9%, as shown in Fig. 4(d). As a comparison, the previously reported highest  $\eta_{pp}$  was only 6.5%, which was mainly attributed to the ultra-high *IPCE* of 900% with photoconductive gains.



**Fig. 4** | (a) EQE characteristics of the QLED based on large CdSe-based quantum dots. (b)  $J$ - $V$ - $L$  characteristics and (c)  $IPCE$  or  $EQE_i$  characteristics of the up-conversion devices integrating the QLED with less efficiency roll-offs. (d) The  $\eta_{pp}$  of (green) up-conversion devices with optimized PbS layers and improved matching between PD unit and QLED unit, (pale red) up-conversion devices before optimization.

## Conclusions

The work mainly provided thorough understanding on the limiting factors to the performances of infrared-to-visible up-conversion devices. One of the main limiting factors was the poor matching between PD unit and QLED unit in up-conversion devices. Though the quantum efficiency of the QLED unit achieved its maximum under low working bias ( $< 6$  V) in up-conversion devices, the effective  $IPCE$  of the PD unit was very low and the integration loss ( $1-\eta_i$ ) was very high, leading to low  $\eta_{pp}$ . The low effective  $IPCE$  originated from the small effective bias allocated onto the PD unit. With low working bias ( $< 6$  V), the photogenerated holes cannot overcome the interconnection barrier. Lots of photogenerated carriers were accumulated and recombined at the interface, leading to high integration loss ( $\sim 80\%$ ) at low working bias. With high working bias ( $\sim 10$  V), the PD unit achieved its maximum  $IPCE$ , while the  $EQE_i$  of the QLED might decrease due to efficiency roll-off, resulting in significant efficiency loss in up-conversion devices. Since the PD unit must achieve high  $IPCE$  under large working bias in up-conversion device, improving the

matching between the PD unit and QLED unit usually rely on using a QLED with minimal efficiency roll-off. This also reminded us that pursuing high maximum EQE in QLEDs under low working bias was meaningless for improving the performance of up-conversion devices. By integrating a QLED with minimal efficiency roll-off, the performances of the up-conversion device improved significantly. On the other hand, the integration losses of the up-conversion devices were still over 65%, no matter we used high-barrier or low-barrier interconnection layers. This significant loss was mainly contributed by the absorption of the visible emission in PbS layers. Reducing the thicknesses of PbS layers brought moderate improvement in  $\eta_{pp}$  of the up-conversion device through a balanced infrared absorption and visible transmission in PbS layers. Finally, the suppressed efficiency roll-off in QLED unit, together with optimized PbS layers, resulted in a breakthrough  $\eta_{pp}$  of 6.9%. More sophisticated optical structure, such as micro-cavity or plasmonic structure, may bring additional room for optimizing the performances of quantum dot-based up-conversion devices.

## Experiments

**Synthesis of infrared PbS quantum dots:** PbS quantum dots, working as the infrared absorber in up-conversion photodetector, was synthesized through the same methods described in our previous work or ref.<sup>30</sup>. In simple terms, the PbO-based Pb-precursor and bis(trimethylsilyl) sulfide were reacted in mixture of oleic acid and 1-octadecene. Then, methanol and acetone were used to purify the original solution of quantum dots. PbS quantum dots with concentration of 50 mg/mL was used for device fabrication.

**Preparation of ZnO and ZnMgO layer:** ZnO sol-gel layer was obtained through blending Zinc acetate dehydrate (0.5 g), ethanolamine (0.135 mL), and 2-methoxyethanol (10 mL) and 12 h vigorous stir in the dark. ZnMgO nanoparticles were synthesized through the same methods described in our previous work or ref.<sup>30</sup>.

**Red emitting CQDs:** CdSe/ZnS with thick shell was purchased from Suzhou Xingshuo Nanotech Co., Ltd. ZnCdSe/ZnS QDs with alloy cores were synthesized in-house. 6 mL bis(trimethylsilyl) selenide and 8 mL paraffin oil were fully mixed in a flask with nitrogen atmosphere and then was heated to 310 °C. For the growth of the red QDs, 2 mL Zn precursor and 0.2 mL Cd precursor were fully mixed before they were injected into the flask, while the temperature was kept at 300 °C during

the 15 min growth. The 4.8 mL mixture of Zn precursor and S precursor with a ratio of 1:1.4 were dropped slowly into the reaction flask so that the temperature was still kept at 300 °C. The solution was cooled down to room temperature as quick as possible at the end of growth. The resulted red QDs were purified with acetone first and then methanol.

**Device Fabrication:** The ITO/glass substrates used for device fabrication were purchased and showed 20  $\Omega$ /sq sheet resistance. The ITO/glass substrates were successively cleaned with deionized water, acetone, and isopropanol for 15 min, followed by 15 min UV-ozone treatment. The layer of sol-gel ZnO contacted with ITO anode was spin coated for 30 s with spin speed of 2000 rpm. The ZnO sol-gel was annealed at 200 °C for 30 mins to obtain ZnO poly-crystal layer. The substrate was wiped using the ethanol to expose the electrode for outer circuit connection. The PbS layer was deposited via layer-by-layer spin coating. For each layer, 40  $\mu$ L PbS solution were spin cast on to the ZnO substrate at 2500 rpm for 20 s. A tetrabutylammonium iodide solution (10 mg/mL in methanol) was then dropped on to the film and left for 30 s, followed by the rinse-spin steps using acetonitrile. This process needs to be repeated 5 times. Then, replaced 1,2-ethanedithiol in acetonitrile solution (0.02 vol%) with tetrabutylammonium iodide solution (10 mg/mL in methanol) and repeated the above process more than twice. The fabrication of QLED started from the deposition of TFB (or PTAA), TFB (or PTAA)/chlorobenzene solution with concentration of 8 mg/mL was spin coated at 4000 rpm for 20 s. The TFB (or PTAA) layer was annealed at 80 °C for 10 mins. Then CdZnSe QDs (18 mg/mL in octane) was spin coated on the substrate at 2500 rpm for 20 s. Then, the top layer of ZnMgO was spin coated at 2000 rpm for 20 s and methylbenzene was used to wipe out the electrodes, then annealed at 80 °C for 10 mins. Finally, the 100 nm top Al-cathode layer was deposited through thermal evaporation in high vacuum chamber. The width of the two orthogonal electrodes determined the light-emitting area, which was 4 mm<sup>2</sup> in our cases. UV curable resin was used to encapsulated the devices before characterizations.

**Device Characterizations:** Absorption and PL spectra were measured by a UV-vis absorption spectrometer (Lambda 950 PerkinElmer spectrometer) and a spectrofluorometer (HORIBA FluoroLog-3), respectively. Transmission electron microscopy (TEM) studies were

performed using a JEOL JEM-2010 electron microscope operating at 200 kV. The current density-voltage-luminance characteristics of the up-conversion devices and QLEDs were measured using a characterization system comprising a Keithley 2400 voltmeter together and a Photo Research 735 spectrometer under ambient conditions. A 980 nm laser was used as the external infrared light source. Capacitance-voltage characterizations were carried out with a Tonghui TH2829C precision LCR meter. The modulating frequency and the modulating amplitude were 100 kHz and 20 mV, respectively.

## References

1. Ban D, Han S, Lu ZH et al. Near-infrared to visible light optical upconversion by direct tandem integration of organic light-emitting diode and inorganic photodetector. *Appl Phys Lett* **90**, 093108 (2007).
2. Gao XH, Cui YY, Levenson RM et al. *In vivo* cancer targeting and imaging with semiconductor quantum dots. *Nat Biotechnol* **22**, 969–976 (2004).
3. Gu YY, Guo ZY, Yuan W et al. High-sensitivity imaging of time-domain near-infrared light transducer. *Nat Photonics* **13**, 525–531 (2019).
4. Zhao YQ, Yang SY, Zhao JS et al. PbS quantum dots based organic-inorganic hybrid infrared detecting and display devices. *Mater Lett* **196**, 176–178 (2017).
5. De Iacovo A, Venettacci C, Colace L et al. PbS colloidal quantum dot photodetectors operating in the near infrared. *Sci Rep* **6**, 37913 (2016).
6. Ng TN, Wong WS, Chabinyo ML et al. Flexible image sensor array with bulk heterojunction organic photodiode. *Appl Phys Lett* **92**, 213303 (2008).
7. Yang Y, Zhang YH, Shen WZ et al. Semiconductor infrared up-conversion devices. *Prog Quantum Electron* **35**, 77–108 (2011).
8. Shen TY, Qin JJ, Bai YJ et al. Giant magneto field effect in up-conversion amplified spontaneous emission via spatially extended states in organic-inorganic hybrid perovskites. *Opto-Electron Adv* **5**, 200051 (2022).
9. Xu KM, Zhou WJ, Ning ZJ. Integrated structure and device engineering for high performance and scalable quantum dot infrared photodetectors. *Small* **16**, 2003397 (2020).
10. Wu ZH, Yao WC, London AE et al. Elucidating the detectivity limits in shortwave infrared organic photodiodes. *Adv Funct Mater* **28**, 1800391 (2018).
11. Wu ZH, Zhai YC, Yao WC et al. The role of dielectric screening in organic shortwave infrared photodiodes for spectroscopic image sensing. *Adv Funct Mater* **28**, 1805738 (2018).
12. Wang WG, Wu ZH, Ye TK et al. High-performance perovskite light-emitting diodes based on double hole transport layers. *J Mater Chem C* **9**, 2115–2122 (2021).
13. He JH. High-performance warm white LED based on thermally stable all inorganic perovskite quantum dots. *Opto-Electron Adv* **6**, 230022 (2023).
14. Lu TW, Lin XS, Guo W et al. High-speed visible light communication based on micro-LED: a technology with wide applications in next generation communication. *Opto-Electron Sci* **1**, 220020

- (2022).
15. Wu ZH, Liu P, Qu XW et al. Identifying the surface charges and their impact on carrier dynamics in quantum-dot light-emitting diodes by impedance spectroscopy. *Adv Opt Mater* **9**, 2100389 (2021).
  16. Wu ZH, Liu P, Zhang WD et al. Development of InP quantum dot-based light-emitting diodes. *ACS Energy Lett* **5**, 1095–1106 (2020).
  17. Liu MX, Voznyy O, Sabatini R et al. Hybrid organic-inorganic inks flatten the energy landscape in colloidal quantum dot solids. *Nat Mater* **16**, 258–263 (2017).
  18. Ning ZJ, Voznyy O, Pan J et al. Air-stable n-type colloidal quantum dot solids. *Nat Mater* **13**, 822–828 (2014).
  19. Wang RL, Shang YQ, Kanjanaboos P et al. Colloidal quantum dot ligand engineering for high performance solar cells. *Energy Environ Sci* **9**, 1130–1143 (2016).
  20. Marus M, Xia Y, Zhong HY et al. Bright infra-red quantum dot light-emitting diodes through efficient suppressing of electrons. *Appl Phys Lett* **116**, 191103 (2020).
  21. Zhang N, Tang HD, Shi KM et al. High-performance all-solution-processed quantum dot near-infrared-to-visible upconversion devices for harvesting photogenerated electrons. *Appl Phys Lett* **115**, 221103 (2019).
  22. Wei YZ, Ren ZW, Zhang AD et al. Hybrid organic/PbS quantum dot bilayer photodetector with low dark current and high detectivity. *Adv Funct Mater* **28**, 1706690 (2018).
  23. Yu H, Kim D, Lee J et al. High-gain infrared-to-visible upconversion light-emitting phototransistors. *Nat Photonics* **10**, 129–134 (2016).
  24. Kim DY, Choudhury KR, Lee JW et al. PbSe nanocrystal-based infrared-to-visible up-conversion device. *Nano Lett* **11**, 2109–2113 (2011).
  25. Tang HD, Shi KM, Zhang N et al. Up-conversion device based on quantum dots with high-conversion efficiency over 6%. *IEEE Access* **8**, 71041–71049 (2020).
  26. Zhou WJ, Shang YQ, García de Arquer FP et al. Solution-processed upconversion photodetectors based on quantum dots. *Nat Electron* **3**, 251–258 (2020).
  27. Lee JW, Kim DY, So F. Unraveling the gain mechanism in high performance solution-processed PbS infrared PIN photodiodes. *Adv Funct Mater* **25**, 1233–1238 (2015).
  28. Shen HB, Gao Q, Zhang YB et al. Visible quantum dot light-emitting diodes with simultaneous high brightness and efficiency. *Nat Photonics* **13**, 192–197 (2019).
  29. Mu G, Rao TY, Zhang S et al. Ultrasensitive colloidal quantum-dot upconverters for extended short-wave infrared. *ACS Appl Mater Interfaces* **14**, 45553–45561 (2022).
  30. Xu QL, Yang XX, Liu JJ et al. Elaborating the interplay between the detecting unit and emitting unit in infrared quantum dot up-conversion photodetectors. *Nanoscale* **15**, 8197–8203 (2023).
  31. Chuang CHM, Brown PR, Bulović V et al. Improved performance and stability in quantum dot solar cells through band alignment engineering. *Nat Mater* **13**, 796–801 (2014).
  32. Kumawat NK, Gupta D, Kabra D. Recent advances in metal halide-based perovskite light-emitting diodes. *Energy Technol* **5**, 1734–1749 (2017).
  33. Bi Y, Pradhan S, Gupta S et al. Infrared solution-processed quantum dot solar cells reaching external quantum efficiency of 80% at 1.35 $\mu\text{m}$  and  $J_{\text{SC}}$  in excess of 34  $\text{mA cm}^{-2}$ . *Adv Mater* **30**, 1704928 (2018).
  34. Vafaie M, Fan JZ, Morteza Najarian A et al. Colloidal quantum dot photodetectors with 10-ns response time and 80% quantum efficiency at 1, 550nm. *Matter* **4**, 1042–1053 (2021).
  35. Würfel U, Neher D, Spies A et al. Impact of charge transport on current-voltage characteristics and power-conversion efficiency of organic solar cells. *Nat Commun* **6**, 6951 (2015).
  36. Neher D, Kniepert J, Elimelech A et al. A new figure of merit for organic solar cells with transport-limited photocurrents. *Sci Rep* **6**, 24861 (2016).
  37. Deng YZ, Lin X, Fang W et al. Deciphering exciton-generation processes in quantum-dot electroluminescence. *Nat Commun* **11**, 2309 (2020).

## Acknowledgements

This work was supported by the following research fundings including: the National Natural Science Foundation of China (Nos. 62005114, 62204078 and U22A2072), Natural Science Foundation of Henan - Excellent Youth Scholar (No. 232300421092), and Open Fund of the State Key Laboratory of Integrated Optoelectronics + (IOSKL2020KF01).

## Author contributions

All authors commented on the manuscript. JJ Liu and XX Yang conducted the experiments including device fabrication and characterization. QL Xu conducted data analysis and also supported device characterization. RG Chang supported device characterization, ZH Wu formulated the research idea, analysed the data, wrote the manuscript, obtained the research funding and supervised the whole work. HB Shen obtained some key resources necessary for doing the research including research funding and platform.

## Competing interests

The authors declare no competing financial interests.

## Supplementary information

Supplementary information for this paper is available at <https://doi.org/10.29026/oes.2024.230029>



Scan for Article PDF